Oil & Gas Science and Technology – Rev. IFP, Vol. 57 (2002), No. 5, pp. 579-590

Simulation of Borehole Breakouts Using FRACOD^{2D}

B. Shen[1], O. Stephansson[2] and M. Rinne[3]

1 CSIRO Exploration and Mining, Kenmore, Brisbane - Australia
2 GeoForschungsZentrum, Potsdam, Germany & KTH, Stockholm - Sweden
3 FRACOM Ltd, Kyrkslätt - Finland
e-mail: baotang.shen@csiro.au - ove@aom.kth.se - mikael.rinne@fracom.fi

Résumé — Simulation des éclatements des trous de forage avec l'utilisation de FRACOD^{2D} — Les éclatements des trous de forage apparaissent souvent avec des mécanismes de panne complexes et les deux ruptures, de traction et de cisaillement, sont concernées. Pour faciliter l'étude du phénomène des défaillances, un nouveau code de propagation des pannes, FRACOD^{2D}, est présenté dans cet article. Le code simule la propagation des avaries dans le mode de traction (mode I), dans le mode de cisaillement (mode II) et dans le mode mixte (mode I + II). Il est capable de prévoir des éclatements de trous de perçage causés par une gamme de mécanismes de pannes.

Le code a été appliqué pour étudier dans un nombre de cas les avaries de perçage avec les différentes valeurs d'effort et de pression des fluides. Il a été observé que, dans la plupart des cas, les avaries de cisaillement sont impliquées dans la formation finale de la défaillance. Les avaries de tension seules ne conduisent pas à la panne. Les modèles numériques ont prévu les pannes typiques en forme de *dog-ear* (oreille de chien). Il a été trouvé que la forme et l'étendue des défaillances (largeur et profondeur) dépendent de la magnitude des efforts appliqués, aussi bien que la pression du fluide dans le trou de forage. Les résultats de modélisation sont cohérents avec les résultats des tests en laboratoire et les observations sur le terrain. Les facteurs affectant les mécanismes de l'avarie sont commentés.

Abstract* — *Simulation of Borehole Breakouts Using FRACOD^{2D} — *Borehole breakouts often occur with complicated failure mechanisms, involving both tensile and shear failures. To facilitate studies on borehole breakout phenomena, a new fracture propagation code FRACOD^{2D} is introduced in this paper. The code simulates fracture propagation in the tensile mode (mode I), shear mode (mode II) and the mixed mode (mode I + II). It is capable of predicting borehole breakouts caused by a range of failure mechanisms.*

The code has been applied to study borehole breakouts in a number of cases with different stress ratios and fluid pressures. It was found that in most cases, shear failures are involved in the final formation of a breakout. Tensile failures alone do not form breakouts. The numerical models predicted the typical "dog-ear" shaped breakouts. The shape and extents of the breakouts (width and depth) were found to depend upon the magnitude of applied stresses as well as the fluid pressure in the borehole. The results of modeling are consistent with laboratory test results and field observations. Factors affecting breakout mechanism are discussed.

INTRODUCTION

Borehole breakouts, *i.e.* failure of the borehole wall due to stress concentrations, result in an elongation of the borehole cross-section in the direction of minimum principal stress. An understanding of the breakout phenomena is important for determining the orientations of *in situ* stresses. The relation between the magnitude of the *in situ* stresses and the width and depth of the breakouts are of particular importance for stress measurement using borehole breakouts.

Previous observations and theoretical analyses of borehole breakouts indicated that failure of borehole wall is often of two different modes governed by either tensile spalling or shear fracturing (Vardoulakis *et al*., 1988; Guenot, 1989). In the case of tensile spalling, the rock breakage starts in the vicinity of a borehole as a result of tensile crack initiation and propagation in the direction of the maximum compressive principal stress. A series of sub-parallel cracks are formed and the coalescence of these tensile cracks makes up a layer which may fall off from the borehole wall. This phenomenon is typical for hard crystalline rocks such as granite under compression with no or small lateral confinement (see *e.g.* Ewy and Cook, 1990a and 1990b; Lee and Haimson, 1993, Martin *et al*., 1994, Haimson and Lee, 1995, Amadei and Stephansson, 1997). In the case of shear fracturing, shear failure along one or more shear bands extends from the borehole wall into the rock. The shear fractures (or shear bands) can cause breakout when they intersect one another. This type of failure is often observed in soft and porous rocks, such as dolomite, limestone and sandstone (Zoback *et al*., 1985; Guenot, 1989). Both failure modes can result in dog-ear shaped breakouts, *i.e.* breakouts with a wider area at the borehole wall and a sharp end in the rock.

Theoretical studies have been conducted to understand and predict the two breakout mechanisms. The breakout by shear was assumed to follow Mohr-Coulomb failure criterion (Zoback *et al*., 1985). This could explain the wide and shallow breakout sometime observed in the field, but not the formation of sharp-edged breakouts of "dog-ear" type.

Extensile cracking has been observed in uni- or bi-axial borehole tests in laboratory. Extensile cracking is attributed to the structure instability of the borehole wall. Vardoulakis *et al*. (1985) and Zheng *et al*. (1989) used a compressive failure criterion with a numerical method and predicted the breakout of "dog-ear" shape as a result of gradual failure. The results provided a close representation of the phenomenon, but could not explain the physical mechanism of extensile cracking.

A fracture mechanics approach was used by Shen *et al.* (1997) to predict the breakouts formed by tensile fracturing and shear fracturing, respectively. Two different numerical models were used to study the breakouts in the two mechanisms with reasonable success.

In a recent study, Haimson (2001) found that in highly porous sandstone, fracture-like failure bands formed in the direction of the minimum principal stress. He explained the failure bands as caused by progressive compaction failure (particle crushing and pore collapses) of the rock material. The mechanism of this type of failure is referred in this paper as "compressive mode", which differs from the shear and tensile modes discussed above.

In this paper, we studied the three borehole failure modes by using the numerical code FRACOD^{2D} developed by Shen (2001). A large number of cases were simulated. The effects of a number of parameters (*e.g.* stress ratio, initial fracture position, fluid pressure in the borehole) on the breakout shape and failure mechanisms were investigated.

1 THE FRACTURE PROPAGATION CODE-FRACOD^{2D}

A two-dimensional boundary element code FRACOD^{2D} has been developed to simulate fracture propagation in an elastic and isotropic rock medium. The code employs the displacement discontinuity method (DDM) and a recently proposed fracture propagation criterion (for detecting the possibility and the path of fracture propagation). The current version of the code is fully Window based and user friendly. The code can simulate up to 10-15 nonsymmetrical, and randomly distributed fractures. The code simulates fracture propagations in a linearly elastic, homogenous and isotropic medium. It predicts fracture process in both mode I (tension), mode II (shear) and mixed mode I + II. Attempts are also made in this paper to use FRACOD^{2D} to predict the "compressive" fracture propagation.

1.1 Fracture Criterion

In nature, rock fractures often initiate and extend in a form of shear, which is not described by the classical mode I fracture criteria. Note that we use the term fracture here for rock discontinuities in macro-scale. Similar to the concept of energy release rate criterion (*G*-criterion), a modified energy release rate criterion—*F*-criterion has been developed (Shen and Stephansson, 1994). In this criterion not only the energy release associated with tensile fracturing, but also that with shear fracturing influence the failure process. The direction and the critical condition of fracture propagation are determined by:

$$F(\theta)\big|_{\theta=\theta_0} = \frac{G_I(\theta)}{G_{IC}} + \frac{G_{II}(\theta)}{G_{IIC}} = F_{\max} \geq 1 \qquad (1)$$

where θ is the direction angle of the fictitious fracture tip to the face of an initial fracture *(see Fig. 1)*; G_I and G_{II} represent the energy release rate by pure tension and pure shear at the fracture tip, respectively. The criterion is capable

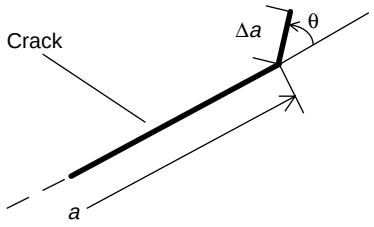

Figure 1

Fictitious crack increment Δa in direction θ with respect to the initial crack orientation.

of predicting both mode I and mode II fracturing. The fracture propagation is simulated numerically by a DDM code implemented with the *F*-criterion (Shen, 1993).

1.2 Numerical Method for Fracture Propagation

The DDM, developed by Crouch (1976), is one of the indirect boundary element methods. Different from the commonly used direct integration method, DDM is based on the solution of a unit displacement discontinuity (*e.g.* crack) in an isotropic and elastic medium. Using this method, the two opposite crack surfaces can be represented by only one element. The displacement discontinuities of the crack element are directly obtained by solving the systematic equations. The solution of a fracture system is more effective and faster than other methods (*e.g.*, finite element method).

The displacement discontinuity, D_i, is defined as the difference in the displacements (u_i) between the two sides of a fracture element.

$$\begin{aligned} D_s &= u_s^- - u_s^+ \\ D_n &= u_n^- - u_n^+ \end{aligned} \tag{2}$$

where *s*, *n* represent shear and normal directions respectively and +, – signs denote the upper and lower surfaces respectively. A system of equations are constructed for D_i (i = *s*, *n*) with specified boundary conditions (Crouch, 1976) and the displacements and stresses can be calculated by solving the system of equations:

$$\begin{aligned} \sigma_s^i &= \sum_j \left(A_{ss}^{ij} D_s^j + A_{sn}^{ij} D_n^j \right) \\ \sigma_n^i &= \sum_j \left(A_{ns}^{ij} D_s^j + A_{nn}^{ij} D_n^j \right) \end{aligned} \tag{3}$$

where A_{ss}^{ij}, etc., are the boundary influence coefficients determined by the elastic properties of the materials and the element geometry. The stresses at the fracture elements meet one of the following conditions:

– $\sigma_s^i = \sigma_n^i = 0$ (open crack)

– $\sigma_s^i = K_s D_s^i$, $\sigma_n^i = K_n D_n^i$ (closed crack)

– $\left|\sigma_s^i\right| = \sigma_n^i \tan\phi$, $\sigma_n^i = K_n D_n^i$ (sliding crack)

where K_s, K_n are the fracture shear and normal stiffness, and ϕ is friction angle of rock.

According to the energy release criterion, a fracture will propagate if:

$$-\frac{d\Pi}{da} \geq G_c \tag{4}$$

Π is the sum of the elastic and potential energy per unit thickness of the plane model and is expressed as:

$$\begin{aligned} \Pi(a) = &-\frac{1}{2}\sum_{i=1}^{m_1} a^i \left(\sigma_s^i D_s^i + \sigma_n^i D_n^i\right) \\ &-\frac{1}{2}\sum_{i=m_1+1}^{m_1+m_2} a^i \left(\sigma_s^i u_s^i + \sigma_n^i u_n^i\right) \end{aligned} \tag{5}$$

where:

m_1, m_2 = total numbers of fracture elements and the geometry boundary elements, respectively;

a^i = length of the ith element.

The energy release rate is hence given by:

$$G = -\frac{\Pi(a + \Delta a) - \Pi(a)}{\Delta a} \tag{6}$$

where Π (a + Δa) is the energy when a fictitious element with a length of Δa is added to the tip element to simulate the potential growth.

The strain energy release rates for mode I and mode II (G_I and G_{II}) in Equation (1) is calculated when the fictitious tip element is restricted in shear and tension, respectively.

2 SIMULATION OF BOREHOLE BREAKOUTS FORMED BY TENSILE SPALLING

In this study, a single borehole in an elastic, homogenous and isotropic rock medium was simulated. Plane strain condition was assumed. The borehole radius was 1.0 m for all cases listed in this study. The rock elastic properties were: Young's modulus (E) = 40 GPa, Poisson's ratio (ν) = 0.25. Different fracture properties were used in this study to investigate different types of failure.

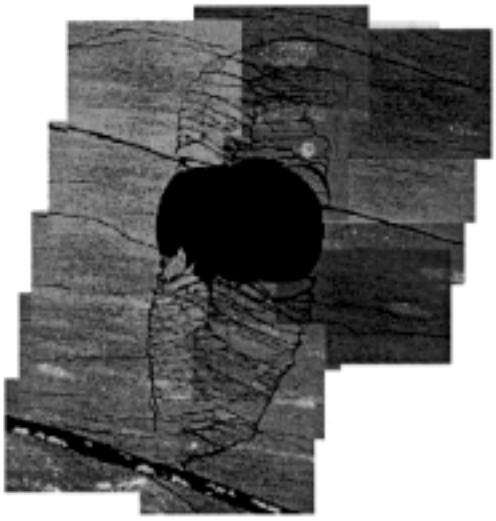

Figure 2

Borehole breakouts caused by tensile spalling. After Germanovich and Dyskin (2000).

The current version of FRACOD^{2D} does not simulate fracture initiation. Therefore, it is necessary to introduce initial fractures in the model. The position and orientation of the initial fractures may affect the modeling results. Hence, a number of different initial fracture geometries were investigated.

The modeling was conducted using symmetry fractures to reduce the calculation time. Nonsymmetry fractures had been found to produce similar but more irregular breakouts.

Tensile spalling is believed to be caused by the extension of wing cracks from existing flaws in the borehole wall and the final buckling failure of thin rock layers (Germanovich and Dyskin, 2000). A typical case of breakouts is shown in Figure 2.

To simulate this type of failure, we introduced a number of inclined fractures in the borehole wall as shown in Figure 3. The fracture surfaces were in contact but had very low friction (it is assumed to be 0). The critical energy release rates for fracture propagation were: G_{Ic} = 10 J/m^2, G_{IIc} = 2000 J/m^2. Uniaxial compressive stress was applied and the fluid pressure inside the borehole was 0.

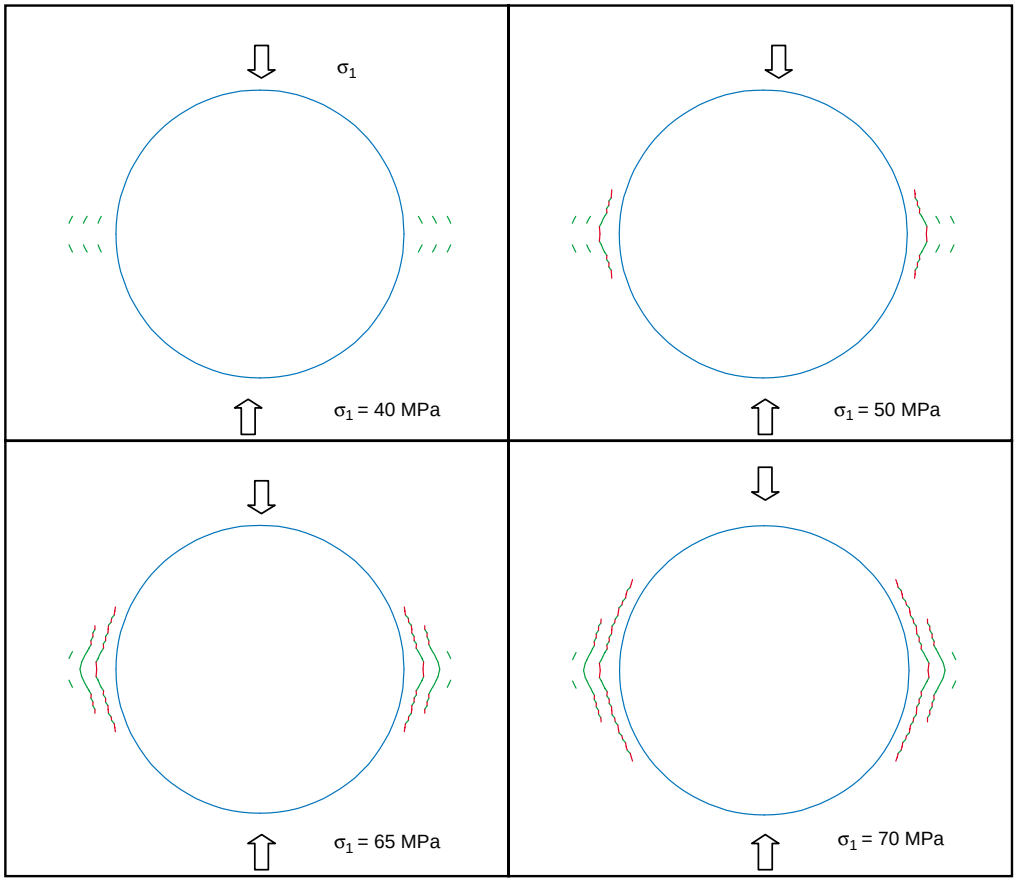

Figure 3

Borehole breakouts dominated by tensile fracture propagation. Colour convention: red: open fracture; green: sliding fracture; blue: elastically contacting fracture.

The modeled process of failure is given in Figure 3 and described as follow. The initial fractures closest to the borehole wall started to propagate at an unaxial stress of 50 MPa. They coalesced and extended in the directions parallel to the borehole wall. Fracture propagation was caused by a combination of tensile failure and shear failure, but dominated by tensile failure. At an unaxial stress of 65 MPa, the initial fractures in the next row started to propagate, also in a mixed mode. At the stress level of 70 MPa, the inner fractures extended to a length of 2/3 of the hole diameter, resulting in a long and thin layer of rock in the borehole wall. It is likely that at this stage buckling failure would have occurred (the code does not model buckling) and hence breakouts were formed.

Although the propagation of fractures was dominated by tensile failure in this case, shear failure played an important role in the path of propagation. When the shear failure was restricted by using a very high G_{IIc}, initial fractures were found to propagate in tension to a very limited distance and then stop. Such a case is similar to that shown in the top-right figure of Figure 3. The pure tensile fractures were often parallel to the direction of maximum loading (vertical in Figure 3) and do not follow the curve of the borehole wall.

In actual rocks where a large number of flaws exist, tensile fracture propagation is likely to link some flaws together and form an extended fracture in the direction of maximum compressive principal stress. However, a critical failure path is often formed due to shear failure, which causes the coalescence of many flaws in the direction of maximum shearing (Shen, 1993).

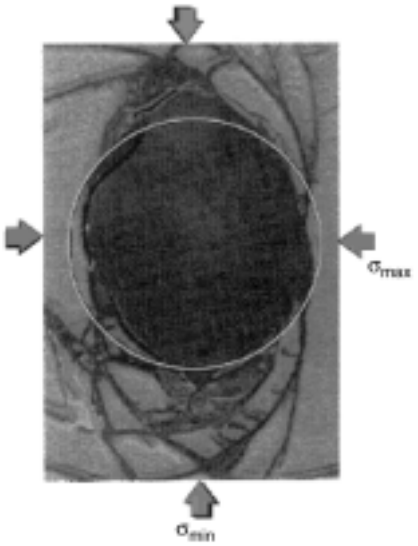

Figure 4

Typical borehole breakouts caused by shear fracturing. After Syarifuddin and Busono (1999).

3 SIMULATION OF BOREHOLE BREAKOUTS FORMED BY SHEAR FRACTURING

Borehole breakouts caused by shear fracturing were often found in the laboratory tests and field observations. A typical case of such breakouts is shown in Figure 4, where shear fractures (or shear bands) propagated and intersected with each other to form the breakouts.

In this numerical study, three cases using different initial fracture geometries were studied. They are listed below:

– case 1, initial fractures parallel to the borehole wall;
– case 2, initial fractures intersecting the borehole wall; and
– case 3, combination of case 1 and case 2.

In this section, a fracture surface friction angle of 30° was used. The critical energy release rates for fracture propagation were: G_{Ic} = 50 J/m^2, G_{IIc} = 1000 J/m^2. Different maximum/minimum principal stress ratios (σ_1/σ_3) and different fluid pressures in the borehole were used.

3.1 Case 1, Modeling with Initial Fractures Parallel to the Borehole Wall

The geometry of the initial fractures is shown in Figure 5 (first picture). Four stress ratios were investigated: σ_1/σ_3 = 1.5; 2.0; 3.0 and 4.0. The two principal stresses were progressively and proportionally increased until failure occurs. Four fluid pressure values were used: σ_p = 0, 5 MPa, 10 MPa, and 15 MPa. The simulation results are discussed below.

3.1.1 Failure Process

A typical breakout process is shown in Figure 5. In this case, the applied stress ratio was σ_1/σ_3 = 2.0 and the fluid pressure in the borehole was 5 MPa.

The failure started at the fractures at an angle of 30° to the borehole centre, when the applied stresses were σ_1 = 63 MPa and σ_3 = 31.5 MPa. The fractures propagated mainly in shear. The extension of these fractures later triggered the growth of other fractures. Finally, fractures coalesced and formed "dog-ear" type of breakouts. The failure process was predicted to be unstable, *i.e.*, they occurred without any increase of stresses.

Limited tensile failure was observed in this process. However, the tensile failure was not crucial to alter the path of fracture propagation and the shape of the breakouts.

3.1.2 Effect of Stress Ratio

The ratio of the maximum/minimum principal stresses was found to have major effect on the shape of the breakouts and the peak stress when the final breakouts formed. Figure 6 shows the final shapes of the breakouts when the stress ratio was σ_1/σ_3 = 1.5, 2.0, 3.0, and 4.0 respectively. At the lowest

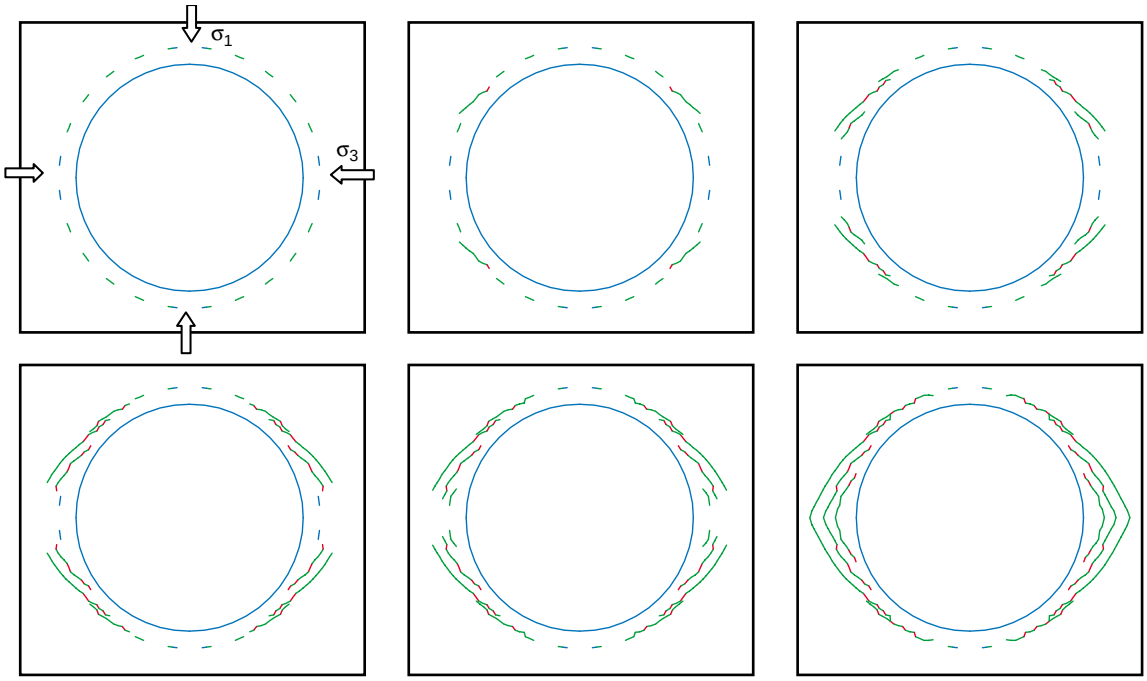

Figure 5

Progressive development of borehole breakouts, dominated by shear fracture propagation. Colour convention: red: open fracture; green: sliding fracture; blue: elastically contacting fracture. σ_1 = 63.0 MPa and σ_3 = 31.5 MPa, fluid pressure σ_p = 5 MPa.

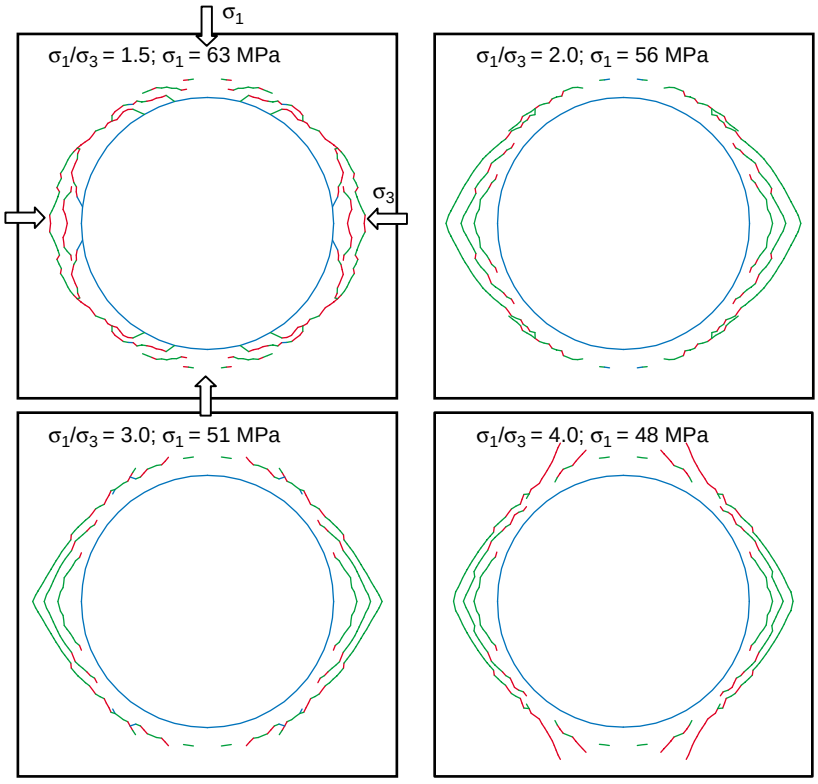

Figure 6

Borehole breakout at different stress ratios. The fluid pressure was 0.

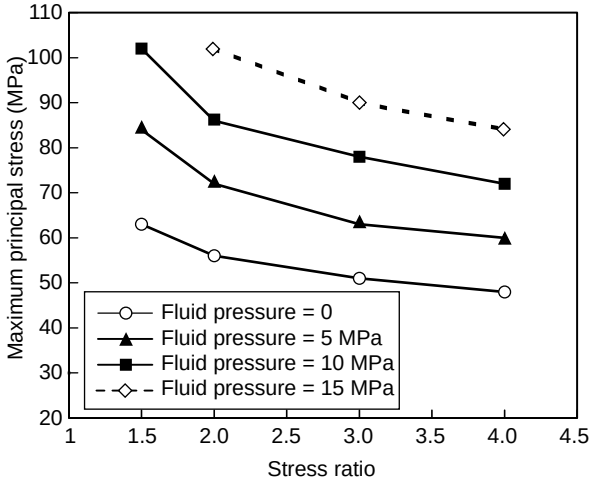

Figure 7

Variation of the peak breakout stress (σ_1) with stress ratios and fluid pressure.

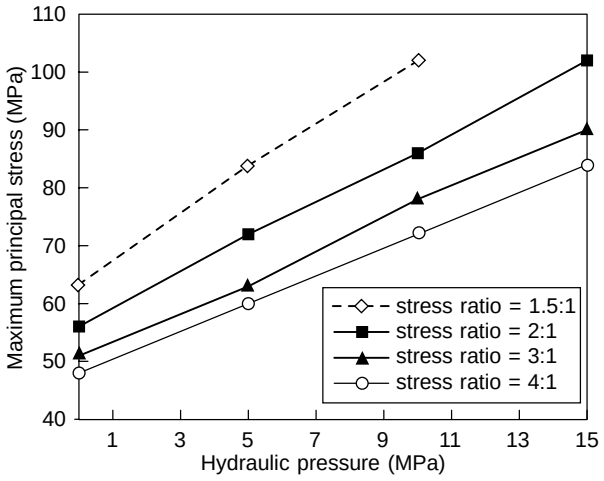

Figure 8

Variation of the peak breakout stress (σ_1) with fluid pressure for different stress ratios.

stress ratio of 1.5, the failure did not form a clear "dog-ear" type of breakouts. Rather, shallow and wide breakouts occurred over much of the borehole wall. At a stress ratios higher than 2.0, typical "dog-ear" breakouts were formed with sharp ends, and the shape was no longer sensitive to the stress ratio. At the highest stress ratio of 4.0, tensile failure occurred above and below the borehole, and extended toward the direction of the maximum compressive principal stress.

The predicted peak breakout stresses decreased with increasing the stress ratio as expected *(Fig. 7)*. The relationship between the peak stress (σ_1) and the stress ratio (σ_1/σ_3) appeared to be nonlinear.

3.1.3 Effect of Fluid Pressure

The fluid pressure in the borehole was found to have minimal effect on the shape of the breakouts for the cases studied. However, increasing fluid pressure would increase the peak breakout stresses (*Fig. 8*). The relationship between the fluid pressure and the peak breakout stresses appeared to be linear. The fluid pressure provides confinement to the rock in a mechanism similar to the triaxial compression tests. In this study, it is assumed that the rock mass is not saturated and fracture surfaces are not subjected to water pressure.

3.2 Case 2, Modeling with Initial Fractures Intersecting the Borehole Wall

Short fractures intersecting the borehole wall were introduced in the numerical model. They may be interpreted to be caused by drilling. The orientation of these fractures varied randomly from 0 to 90° from the tangential direction of the borehole wall. All together 9 cases with different fracture geometries were modelled. Only the stress ratio of $\sigma_1/\sigma_3 = 3.0$ was used. The fluid pressure in the borehole was: $\sigma_p = 5$ MPa.

The shape of the breakouts was found to depend on the orientations of the initial fractures. In some case, shallow and wide breakouts occurred, whereas in other cases deep and pointy breakout were formed, see Figure 9. Statistically, however, there was a linear relation between the extent of breakouts (width and depth) and magnitude of the applied stresses. This relationship is plotted in Figure 10. In Figure 10, the extent of breakout is categorised as:

– breakouts = 1/4 of the borehole boundary, depth = 1/4 of the borehole radius;
– breakouts = 1/3 of the borehole boundary, depth = 1/3 of the borehole radius;
– breakouts = 1/2 of the borehole boundary, depth = 1/2 of the borehole radius.

3.3 Case 3, Modeling with Combined Initial Fractures of Case 1 and Case 2

Two additional simulations were conducted using the combined initial fractures in case 1 and case 2. The modeling results are given in Figure 11. The breakouts were mainly caused by the propagation of the initial fractures parallel to borehole wall.

Consequently, the shape and extent of the breakouts were similar to those of case 1 (using initial fracture parallel to the borehole wall). The peak breakout stress (σ_1), however, was less than that of case 1. The peak breakout stress in (b) and (c) of Figure 11 was 51 MPa and 56 MPa respectively. These

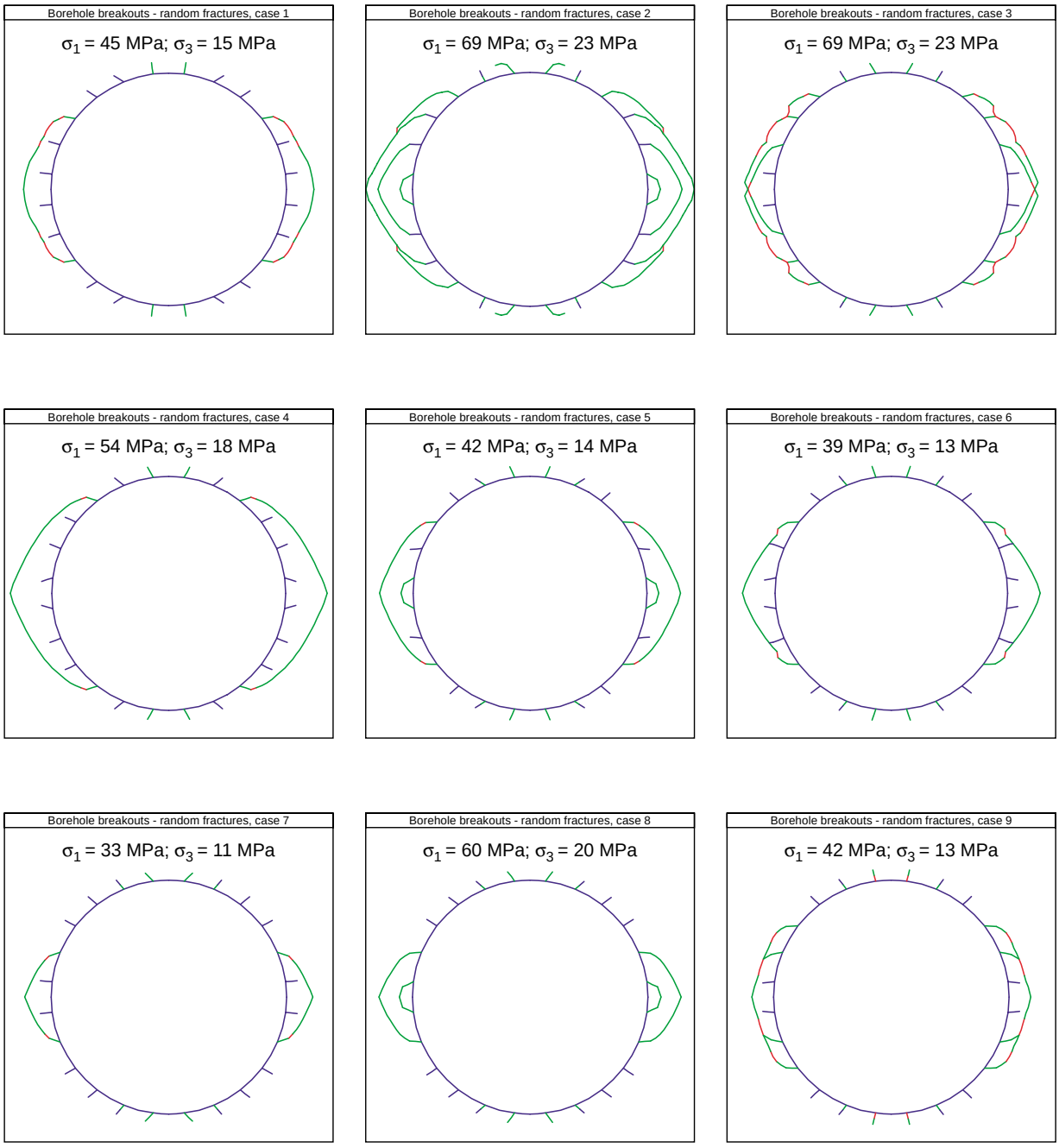

Figure 9

Borehole breakouts formed from random initial fractures intersecting the borehole. Nine cases with random orientations of the initial fractures are presented. The fluid pressure was 5 MPa and the stress ratio of 3 was used.

values are compared with the peak stress of 62 MPa and 72 MPa in case 1 for the same stress ratios. It is believed that the initial fractures intersecting the borehole wall (from case 2) had helped in the breakout process. No cases in case 2 with identical initial boundary fractures were modeled. Therefore, direct comparison with case 2 was not made.

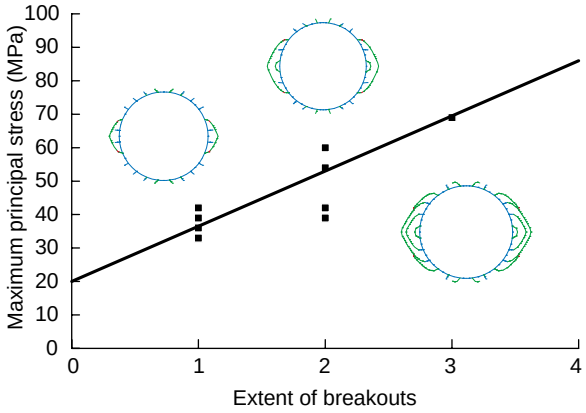

Figure 10

Static variation of the peak breakout stress (σ_1) against the extent of breakouts. Typical breakout shapes are given in the figure. Stress ratio (σ_1/σ_3) was 3.0 and fluid pressure (σ_p) was 5 MPa.

4 SIMULATION OF BOREHOLE BREAKOUTS FORMED BY COMPRESSIVE FAILURE

An attempt was made to simulate the "compressive" borehole breakouts observed by Haimson (2001) using FRACOD^{2D}. The observed breakouts from laboratory experiments are shown in Figure 12. Compact failure bands occurred in the direction perpendicular to the maximum compressive principal stress. Haimson (2001) interpreted this type of failure as due to the pore collapse and particle crushing (compaction) in the highly porous rock material. Other rock characterisations such as compressive/tensile strength ratio etc may also have contributed to this unique phenomenon, and the "compressive" fracturing is still not fully understood.

To model the "compressive" breakouts, FRACOD^{2D} needed to be modified slightly. The original code assumed that the "fictitious" element added to a fracture tip to calculate G_I and G_{II} is nondeformable except when it is found to open or slide. This means that no normal or shear deformation is allowed if this element is in surface closure. For compression type of failure, however, deformation may occur due to the collapse of pores and particles (or compaction). For this reason, we introduced a normal and shear contact stiffness (k_s and k_n) to the "fictitious" tip element. The shear and normal displacements, d_s and d_n of this element are proportional to the shear and normal stresses, *i.e.*

$$d_s = \frac{\sigma_s}{k_s} \qquad d_n = \frac{\sigma_n}{k_n}$$

The displacements represent the total displacements occurred within the "compaction band" at the tip. They are

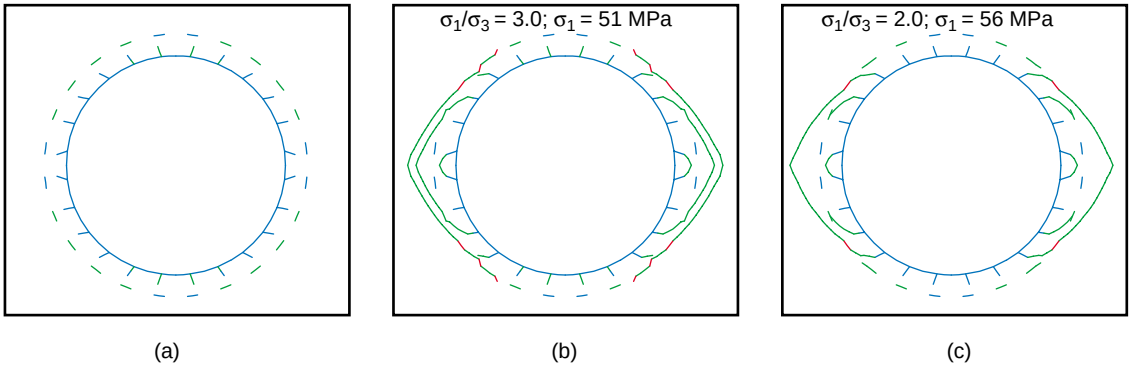

Figure 11

Modeled breakouts using combined initial fractures. Fluid pressure is 5MPa. Results from two stress ratios are presented. (a) initial fracture geometry; (b) modeling results at a stress ratio of 3.0; (c) modeling results at a stress ratio of 2.0.

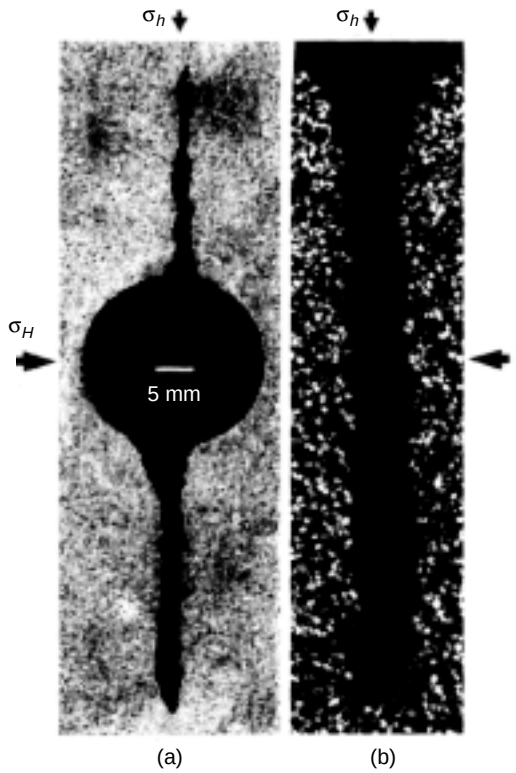

Figure 12

Fracture-like breakouts in porous sandstone caused by "compressive" failure. After Haimson (2001).

inelastic displacement although they were modeled here as elastic displacements using the above equations for simplicity. The same fracture criterion used in the original code to determine both the direction and the stress of fracture propagation was used in the modified FRACOD^{2D}, i.e. when the strain energy release rates due to the deformation of the "fictitious" element is greater than the critical strain energy release rates, fracture propagation occurs.

An example case was modelled as shown in Figure 13. Two initial fractures parallel to σ_3 were introduced in the borehole wall. The stiffnesses of the "fictitious" element are given as:

$$k_s = 500 \text{ GPa/m} \qquad k_n = 500 \text{ GPa/m}$$

Note that in previous cases the "fictitious" element was nondeformable and very high stiffness values ($k_s = k_n = 10^{11}$ GPa/m) were used.

Uniaxial compressive stress was applied to the model and the fluid pressure was 0.

At a stress level of σ_1 = 50MPa, the initial fractures were predicted to propagate in the direction perpendicular to the maximum compressive principal stress. They stopped at a distance about 1/3 of the hole diameter from the borehole wall.

The treatment of rock "compaction" deformation in the model was artificial and improvements were required to simulate the process more realistically. Nevertheless, the modeling results from the simple model appeared to be consistent with the observation made by Haimson (2001). This suggested that FRACOD^{2D} has the potential also to simulate the "compressive" fracture process.

DISCUSSION

The fracture propagation code FRACOD^{2D} was used to model three mechanisms of borehole failure. The numerical models gave fairly reasonable prediction of the fracture phenomena for borehole breakouts. When the tensile spalling type of breakouts was simulated, initial fractures were predicted to propagate following the curvature of the borehole wall. The process was dominated by tensile failure. However, shear failure also played an important role in defining the path of the fracture propagation. The formation of breakouts was likely to occur when the fractures extended longer enough to cause buckling failure of the thin rock layers. When the shear-induced breakouts were simulated, shear fractures grown from and/or within the borehole wall and finally coalesced with each other to form typical "dog-ear" shaped breakouts.

Attempts were also made to use FRACOD^{2D} to simulate the "compressive" type of breakouts observed by Haimson (2001). A simplified stress-displacement relation was used to consider the "compaction" deformation at the fracture tip. The numerical code predicted realistic results, suggesting that the FRACOD^{2D} has the potential to simulate the "compressive" fracture process. However, a better method of simulating the compaction and crushing process of the tip element is required.

Results of the simulation showed that the breakouts formed by the tensile spalling or the shear fracturing can have different shapes. Breakouts formed by extensile cracks were often shallow and had smooth bottom, while shear induced breakouts were deep and often had sharp ends. The stress ratio was found to affect size of the breakouts. At a stress ratio greater than 2.0, the stress ratio did not affect the shape of the breakouts. Laboratory study by Haimson and Lee (1995) revealed distinct and sharp breakouts in specimens of Lac du Bonnet granite. The size of the breakouts increased with σ_H and the shape of the breakouts remained similar, independent of the state of far-field stresses.

The modeling results also showed that, shear fracturing played a key role in the final formation of the breakouts, even when the dominant mechanism of the failure was tension. Shear fracturing was likely to be a common phenomenon for macro-scale failure mechanisms.

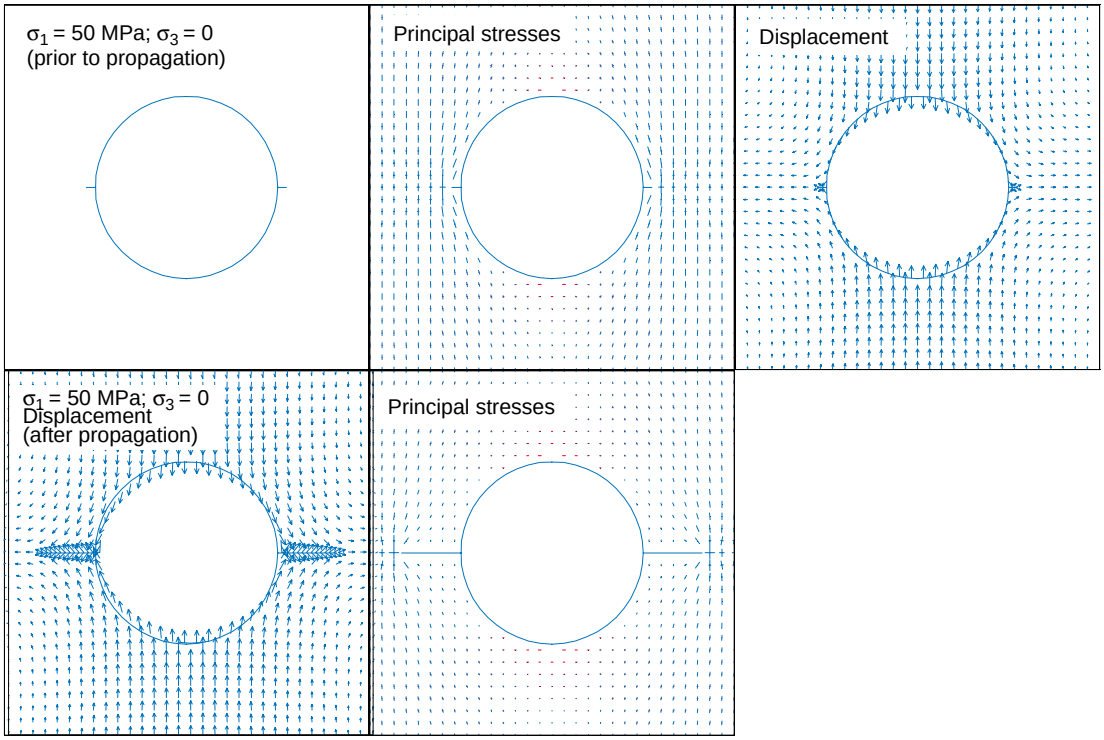

Figure 13

Simulation of the "compressive" fracture propagation using FRACOD^{2D}.

Obviously, borehole breakouts can form in tensile spalling, shear fracturing, or the recently discovered "compressive" fracturing. Discussions are still ongoing about what controls the mechanism of a breakout-material behaviour, stress state or others? It is believed that material behaviour is one of the most important factors to control the mechanism and final shape of borehole breakouts. Rocks are a group of material which can fail both in tension and shear. Highly porous rocks can also fail in compression due to pore collapse and particle crushing. It is a common knowledge that, in laboratory uniaxial tests, some rocks fail in splitting whereas some fail in shear. The failure mode in uniaxial testing is likely to mimic the mechanism of borehole breakout in the same type of rock, since the rock in the wall of the borehole is under almost uniaxial or biaxial stress state.

It has been argued that the mode of breakouts is associated with ratio of compressive strength to tensile strength, σ_c/σ_t, and that shear fracturing is easier to occur in porous material (Vandoulakis *et al.*, 1988; Guenot, 1989; Shen, 1993). Extensile cracking is inhibited under confined condition (Horri and Nemat-Nasser, 1985; Li, 1995). The micro-structures of rocks are often different, some having densely packed particles or minerals and some having relatively loosely cemented particles. The size and distribution of microcracks or voids inside the rock plays an important role in the formation of the failure and hence the breakout formation. Large but loose microcracks are more likely to form splitting as they propagate in tension in the direction of maximum compressive principal stress; small but dense microcracks (voids) intend to form shear failure as they are easier to coalesce in the direction of maximum shearing. This may explain why more shear-induced breakouts were observed in rock types such as sandstone (Rawlings *et al.*, 1993; Kutter and Rehse, 1996).

The "compressive" fracturing is still not fully understood, although the particle collapse and/or pore collapse in highly porous material is believed to be the main causes of this type of breakouts. Further experimental and numerical studies are required to investigate the process of "compressive" fracturing.

CONCLUSIONS

The fracture propagation code FRACOD^{2D} has been demonstrated to predict borehole breakouts formed in complicated failure mechanisms. It provides a useful tool for studying the borehole breakout phenomena.

The modeling results indicated that, in both breakout mechanisms (tensile or shear), shear failures are involved in the final formation of a breakout. Tensile failures alone do not form breakouts. The numerical models also predicted that the shape and extents of the breakouts (width and depth) depend upon the magnitude of applied stresses as well as the fluid pressure in the borehole. The results of modeling are consistent with laboratory test results and field observations.

ACKNOWLEDGEMENTS

This paper was reviewed by H. Guo, D. Adhikary and M. Kelly. Their valuable comments and suggestions are gratefully acknowledged.

REFERENCES

Amadei, B. and Stephansson, O. (1997) *Rock Stress and Its Measurement*, Chapman & Hall, London.

Crouch, S.L. (1976) Solution of Plane Elasticity Problems by the Displacement Discontinuity Method. *Int. J. Num. Methods Engng.*, **10**, 301-343.

Ewy, R.T. and Cook, N.G.W. (1990a) Deformation and Failure around Cylindrical Openings in Rock I. Observations and Analysis of Deformations. *Int. J. Rock Mech. Min. Sci. & Geomech. Abstr.*, **27**, 387-407.

Ewy, R.T. and Cook, N.G.W. (1990b) Deformation and Failure around Cylindrical Openings in Rock II. Initiation, Growth and Interaction of Fracutes. *Int. J. Rock Mech. Min. Sci. & Geomech. Abstr.*, **27**, 409-427.

Germanovich, L.N. and Dyskin, A.V. (2000) Fracture Mechanisms and Instability of Openings in Compression. *Int. J. Rock Mech. Min. Sci.*, **37,** 263-284.

Guenot, A., 1989. Borehole Breakouts and Stress Fields. *Int. J. Rock Mech. Min. Sci. & Geomech. Abstr.*, **26**, 185-195.

Haimson, B.C. and Lee, M.Y. (1995) Estimating *in situ* Stress Conditions from Borehole Breakouts and Core Disking Experimental Results in Granite. In: *Int. Workshop on Rock Stress Measurement at Great Depth*, Sept. 30, Tokyo, Japan, 19-24.

Haimson, B.C. (2001) Fracture-Like Borehole Breakouts in High-Porisity Sandstone: Are they Caused by Compaction Bands? *Phys. Chem. Earth (A)*, **26**, 1-2, 15-20.

Horri, H. and Nemat-Nasser, S. (1985) Compression Induced Microcrack Growth in Brittle Solids: Axial Splitting and Shear Failure. *J. Geophy. Res.*, **90**, B4, 3105-3125.

Lee, M.Y. and Haimson, B.C. (1993) Laboratory Study of Borehole Breakouts in Lac du Bonnet Granite: A Case of Extensile Failure Mechanism. *Int. J. Rock Mech. Min. Sci. & Geomech. Abstr.*, **30**, 1039-1045.

Li, C. (1995) Micromechanics Modelling for Stress-Strain Behaviour of Brittle Rocks. *Int. J. for Num. & Anal. Meth. in Geomech.*, **19**, 331-344.

Kutter, H.K. and Rehse, H. (1996) Laboratory Investigation of Factor Affecting Bborehole Breakouts. *Eurock'96*, Barla (ed.), Balkema, Rotterdam, 751-758.

Martin, C.D. Martino, J.B. and Dzik, E.J. (1994) Comparison of Borehole Breakouts from Laboratory and Field Tests. In: *Proceeding on Rock Mechanics in Petrolum Engineering*, Delft, Balkema, Rotterdam, 183-190.

Rawlings, C.G., Barton, N.R., Bandis, Addis, M.A. and Gutierrez, M.S. (1993) Laboratory and Numerical Discontinuum Modelling of Wellbore Stability. *J. Pet. Technol.*, **45**, 1086-1092.

Shen, B. (1993) Mechanics of Fractures and Intervening Bridges in Hard Rocks, *PhD Thesis*, Royal Institute of Technology, Stockholm, Sweden.

Shen, B. (2001) *FRACOD^{2D} – User's Manual*, Fracom Ltd.

Shen, B. and Stephansson O. (1994) Modification of the G-Criterion for Crack Propagation Qubjected to Compression, *Engng. Fract. Mech.*, **47**, 2, 177-189.

Shen, B., Tan, X., Li, C. and Stephansson, O. (1997) Simulation of Borehole Breakout using Fracture Mechanics Models. In: *Rock Stress*, Sugawara & Obara (eds), 1997 Balkema, Rotterdam. 289-298.

Syarifuddin, N. and Busono, I. (1999) Regional Stress Alignments in the Kutai Basin, East Kalimantan, Indonesia: A Contribution from a Borehole Breakout Study. *Journal of Asian Earth Sciences*, **17**, *123-135.*

Vardoulakis J., Sulem, J. and Guenot, A. (1988) Borehole Instabilities as Bifurcation Phenomena. *Int. J. Rock Mech. Min. Sci. & Geomech. Abstr.*, **25**, 159-170.

Zheng, Z., Kemeny, J. and Cook, N.G.W. (1989) Analysis of Borehole Breakouts. *J. Geophy. Res.*, **94**, B6, 7171-7182.

Zoback M. D., Mooss, D., Mastin, L. and Anderson R. (1985) Wellbore Breakout and *in situ* stress. *J. Geophys. Res.*, **90**, B7, 5523-5530.

Final manuscript received in June 2002